

THE ZEUS EXPERIMENT AT HERA 2002

Proposal 760

**Bristol, Glasgow, Imperial College London, University College London, Oxford,
Rutherford Appleton Laboratory**

in collaboration with

Aegean, Andrews, Argonne, Bologna, Bonn, Calabria, Chonnam, Columbia, DESY, DESY-Zeuthen, Florence, Freiburg, Hamburg, Jülich, Kazakhstan, KEK, Krakow, Kyungpook, Louvain, Madrid, McGill, Moscow, NIKHEF, Ohio, Padova, Pennsylvania, Rome, Santa Cruz, Seoul, Siegen, Tel Aviv, Tokyo, Tokyo Metropolitan Univ., Torino, Toronto, Warsaw, Weizmann Inst., Wisconsin, Yale, York (Ontario).

1 Introduction and Outlook

The year 2002 has been a frustrating one for all experimental groups working at HERA. While there are clear indications from the accelerator side that the essentials of the upgrade to the HERA collider are working, the much higher than expected levels of background that both H1 and ZEUS have experienced have prevented much new data being accumulated for physics analysis. A very large effort from the collider experimental teams and HERA accelerator experts, with full backing from the DESY Directorate, has been directed at understanding the nature of the background and developing solutions to solve or ameliorate the problems. UK members of ZEUS, particularly those resident at DESY with responsibility for the Central Tracking Chamber, have played a crucial role in these studies. While there is still much work to be done a lot has been learnt. At the HERA Coordination Meeting in October it was decided to spend a significant fraction of the months between then and a planned shutdown starting at the beginning of March 2003 on stable running. Even though conditions are far from ideal, this has allowed some 'physics quality' data to be collected. This is very important as it is providing data with which the new ZEUS components can be understood and commissioned for physics analyses under operational conditions.

During the shutdown next year, which will probably last around four months, a number of modifications will be made to collimators and other components in and near the ZEUS interaction region with the aim of reducing the impact of the large backgrounds in the detector. After that the high luminosity physics programme will be resumed.

The UK continues to take responsibility for a wide range of activities within the ZEUS collaboration: the ZEUS spokesman is a UK physicist (to the end of 2002); the UK continues to provide the ZEUS tracking coordinator, the Monte Carlo coordinator, the CTD coordinator; UK physicists are joint coordinators for three of the five ZEUS physics groups.

Sections 2-5 of the report cover the status of the hardware that ZEUS UK is either responsible for or involved with, physics analysis topics are covered in section 6 and factual information on theses, publications and talks is given in the appendices.

2 Central tracking detector status and infrastructure

The Central Tracking Detector (CTD) is a large-volume, cylindrical drift chamber covering the central region ($15^\circ < \theta < 164^\circ$). It provides charged-particle tracking, momentum measurement and identification through dE/dx . It has been installed and operating successfully for 10 years. It also participates in all three levels of the ZEUS trigger.

The CTD's 4608 sense wires are arranged in nine superlayers, superlayer one being the innermost. The wires in odd-numbered superlayers run parallel to the chamber axis, whilst those in even-numbered layers have a small stereo angle ($\approx 5^\circ$). Taken together they provide sufficient information to reconstruct tracks in three dimensions. All sense wires in the chamber are equipped with Flash Analogue-to-Digital Conversion (FADC) electronics and, in addition, all wires in superlayer one and the odd-numbered wires in superlayers three and five have z -by-timing electronics for the first-level trigger.

The CTD has been one of the few components that can provide information on the nature of the backgrounds. In the middle two quarters of the year many special runs were undertaken to diagnose the nature of the backgrounds. During these activities, to ensure the safe operation of the CTD, it was operated only by the CTD experts with around-the-clock coverage. In addition, because of the unusual nature of the analysis, a rather small number of people had to dedicate a large fraction of their time to these tasks. For most of the last quarter of the year, something approaching normal data taking has been achieved. During this period, in order to be able to operate the CTD at the higher beam currents expected from the machine, it was decided to operate the CTD at 95% of the standard HERA-I high voltage settings. The chamber has functioned reliably throughout the year and work is underway to review, and if necessary revise, the various default expectations for track-finding efficiencies and resolutions.

The continued operation and reliability of the CTD is of the utmost importance to the ZEUS experiment physics programme, and will remain so for the remainder of HERA running.

2.1 Triggering

ZEUS operates a three-level trigger, of which the first is a hardware-based system whose principal aim is to reduce backgrounds that do not come from the interaction point. CTD information is essential for this and the detector uses dedicated, pipelined processor cards which provide tracking information to the global first-level trigger. Because of the higher level of background the track triggers are of even greater importance than before. The first level track trigger continues to operate successfully and has not had to be modified.

At the second level more precise software algorithms are used to clean the event sample further and classify certain types of physics events. Detailed tracking information is provided by the CTD second-level trigger which makes use of the data from all five axial superlayers and the z -by-timing information from layers 1, 3 and 5. It is at this level that the biggest changes to the trigger are being made, to take advantage of the extensions to ZEUS tracking (MVD and Forward Tracking) and the price-performance of PC hardware. Before the shutdown for the HERA upgrade, modifications were made to the CTD Transputer network in order to allow data from the FADC electronics to be sent to the new Global Tracking Trigger (GTT). The GTT hardware consists of Gigabit ethernet communications and a farm of 12 1GHz Linux PCs for processing. This augments the original CTD second level transputer based system and the farm hardware has been funded through the Yale ZEUS group. The hardware is working and primary algorithms tested, but until stable data taking conditions are established it will not be used in 'active mode'.

2.2 Infrastructure and Monitoring

Good use was made of the long shutdown for the upgrade to review and repair many of the systems required to keep the CTD operational (gas, water cooling, HV, data acquisition and readout electronics) and a rolling programme of regular maintenance and repair has continued throughout 2002.

The operation of the CTD is checked online by the ZEUS shift crew who have a small number of critical histograms to watch. More detailed monitoring is performed off-line by automatic

analysis of data samples which are then checked by a small team of experts. This procedure has been used for a number of years and has proved effective in the early diagnosis of problems. The system has now been ported to the new ZEUS Linux-based processor farm. It has continued to be important in checking the operation of the CTD and in understanding its performance under the currently rather difficult conditions with a high level of background from HERA.

3 HERA Background Studies

Because of a number of unrelated problems with the HERA collider, it was not until early in 2002 that it became clear that the backgrounds in the ZEUS detector were something like a factor 10 times larger than had been anticipated. It then required intense activity and close collaboration between the experimental groups and HERA machine physicists to pin down both the type and source of the backgrounds. There appear to be at least three different components to the problem:

- off-momentum positrons in time with the positron beam;
- indirect synchrotron radiation back-scattered from an absorber about 11 m on the upstream proton side of the ZEUS interaction point;
- a very large increase in proton beam-gas background, probably due to poor vacuum in the region immediately surrounding the interaction region.

The CTD has been an essential tool in arriving at this point. It was expected that the backgrounds would inevitably be higher after the upgrade, particularly a higher level of synchrotron radiation caused by the more intensely focused beams and new optics needed for HERA-II. New interaction region collimators were designed to avoid any direct synchrotron radiation reaching the sensitive components of the detector. In this they have been successful, unfortunately a rather large amount of radiation back-scattered from the main absorber 11 m from ZEUS is hitting the collimator nearest to the MVD and being scattered into the CTD. It was also expected that the vacuum in and around the interaction point would be worse because the new final-focus superconducting magnets, positioned just inside the ZEUS calorimeter on both sides, do not allow space for as many high-vacuum pumps as before. However the vacuum appears to be something like a factor 8 times worse than expected. The combination of a narrower beam pipe, cold surfaces, more collimators, fewer pumps and new optics is providing a very difficult problem to solve. Ways to alleviate the synchrotron radiation problem by redesigning the nearest collimator and improving the anti-reflection coating on the absorber are well in hand and will be implemented during the shutdown in 2003. More work is needed before then to confirm the vacuum data and come up with a solution.

4 ZEUS Microvertex Detector

To match the upgrade of HERA, ZEUS has upgraded its luminosity monitors, forward tracking and added a silicon strip MicroVertex Detector (MVD). ZEUS UK groups have only been involved in the MVD project with responsibility on the hardware side for: installation; clock and control electronics; the laser alignment system and a cable 'patchbox'. On the software side the local run control, event display and histogramming package were provided by UK people and UK people have a leading role in the development of the second-level global track trigger algorithm and software. We are also involved in offline precision alignment using track data.

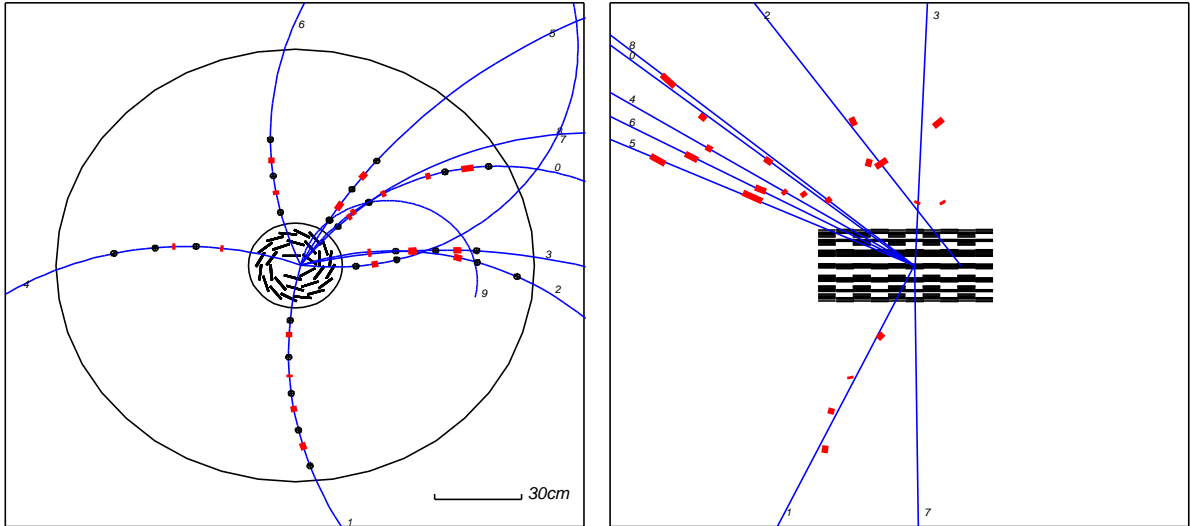


Figure 1: A high transverse energy photoproduction event reconstructed online with the current “CTD-only” GTT algorithm.

4.1 Laser Alignment

The final set of production lasers and the complete VME readout electronics for the MVD alignment system were installed in January 2002. The system has been fully integrated into the MVD slow control system and regular runs performed throughout the year. It showed that the MVD was not disturbed when a thin strip of lead was inserted between the beampipe and MVD radiation shield as part of the background studies. Procedures for analysing the alignment data and establishing stable periods for offline track alignment are being developed.

4.2 Global Track Trigger

The Global Track Trigger (GTT) is a new trigger component for ZEUS. It combines the information from the existing, transputer based, readout systems for the CTD and STT with that from the new, VME based, readout system of the MVD as early as possible in the ZEUS trigger chain. ZEUS-UK are providing the algorithm development, implementation and evaluation, and have been leading the study of the performance of the GTT system as a whole.

Previous studies of the GTT latency were made possible by the implementation of a *playback* system, whereby simulated events could be injected into the GTT trigger chain at the VME component interfaces and then sent through the GTT systems and algorithm processes exactly as for real data. Using simulated high transverse energy photoproduction events, with this system, the deadtime in the ZEUS trigger chain was seen to be below 2% for an input rate to the ZEUS global first level trigger of 400 Hz.

With the advent of dedicated luminosity running since October, it has been possible to test the performance of the GTT on real ep collision data. Since this time, the GTT systems have been seen to run smoothly, with the event distribution and algorithm running continuously in long physics runs.

However, the much larger than expected level of beam gas events originating in or near the interaction region has lead to problems with latency for the ZEUS trigger systems as a whole, and particularly the GTT. Beam gas events typically contain a very large number of tracks so that the occupancy of both the CTD and MVD is very high. Since the GTT must analyse all events from the first level trigger this has significant consequences for the GTT readout systems which are very sensitive to the readout data volume. The need for effective rejection of beam gas events in the GTT was always envisaged, but was not expected to be a problem for the present

lower beam currents. The required layering of the algorithm and tuning of the thresholds in the data transferred to the GTT system has therefore been given a higher priority than originally planned at this stage.

As an intermediate, temporary solution to reduce the deadtime due to beam gas events in the the GTT readout, it has been decided not to send the MVD data to the GTT. At present, this has no negative impact, since the algorithm is currently operating in “CTD only” mode. This is because the MVD is currently in the commissioning stage and the noise occupancy of the MVD is not yet well enough understood to enable the data to be used online. With this modification the deadtime due to the GTT is reduced to below 5%, and studies of the thresholds in the data transferred to the GTT have enabled the deadtime to be reduced to around 1.5% with a latency distribution well within that of the existing CTD second level trigger and essentially no loss in the reconstruction of physics events.

A high transverse energy photoproduction event reconstructed online by the GTT is shown in Fig. 1. Figure 2 shows the z position of the vertex reconstructed by the third level trigger (TLT) and GTT for some recent physics runs. The left plot shows the TLT vertex position for all events which pass the current third level trigger selection (dashed histogram), and events where the reconstructed GTT z position is within ± 20 cm of the nominal interaction point (solid histogram).

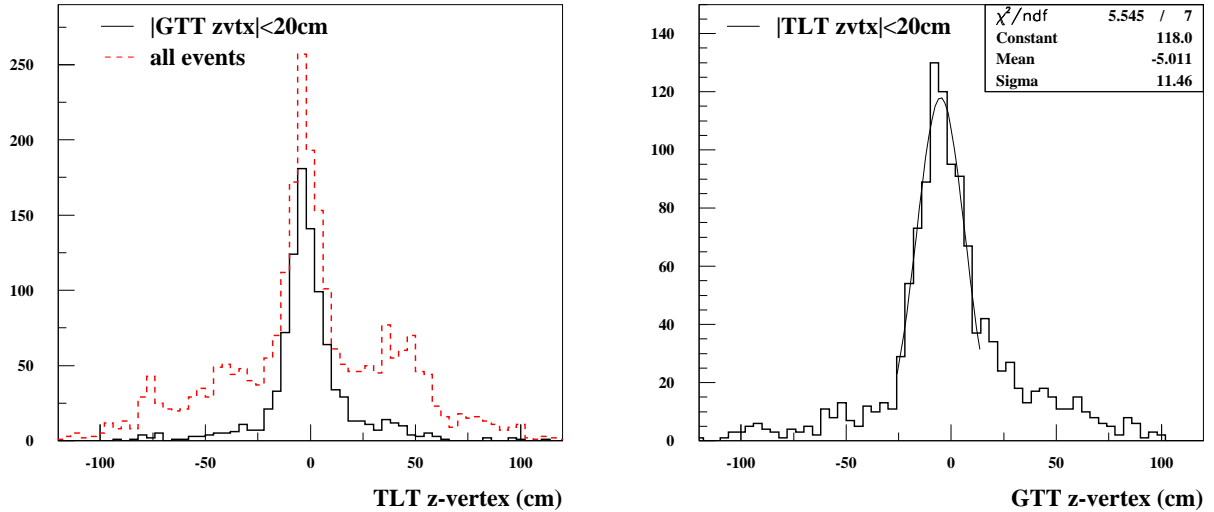


Figure 2: The z -vertex position from the TLT and GTT; left, the TLT vertex for all events written offline (dashed histogram) and those additionally with a vertex reconstructed with the GTT within ± 20 cm of the nominal interaction region; right, the GTT vertex for events with a TLT vertex within ± 20 cm. The expected width of the beam spot, due to the proton bunch length is around 10 cm.

Events passing the third level trigger have been more completely reconstructed than at the GTT stage, and so would be expected to contain fewer background events. However, it is clear that events passing the TLT still contain a significant level of beam gas contamination. By restricting the sample to only those events with a central GTT vertex, the beam gas contribution is significantly reduced with essentially no loss of ep interactions with vertices in the central peak. The right plot shows the GTT vertex position for events with a central vertex from the TLT. The width is consistent with the vertex width due to the proton bunch length.

5 The HERA Polarimetry Upgrade

5.1 Overview

One of the most important objectives of the HERA-II physics programme is the systematic study of the dependence of the neutral and charged current deep inelastic scattering cross sections on the polarisation of the lepton beam. These measurements require a high degree of lepton-beam polarisation and excellent precision on the polarisation measurement (better than 1%). For this purpose a polarimetry upgrade project was set up in 1999; the POL2000 project.

5.2 Polarization Measurement at HERA

At HERA leptons become naturally transversely polarised through the emission of synchrotron radiation (lepton spin flips; Sokolov-Ternov effect). The lepton beam transverse polarisation is converted into longitudinal polarisation near the interaction points by spin rotators. The HERA ring polarisation is measured by two polarimeters: TPOL – the transverse polarimeter which measures transverse polarization, located in the HERA-West area close to HERA-B; and the LPOL – the longitudinal polarimeter which measures longitudinal polarisation, located in the HERA-East area close to HERMES. The degree of polarisation is measured by scattering alternately right- and left-circularly polarised laser light off the polarised lepton beam. The back-scattered Compton photons that are produced are then detected by a calorimeter. The two polarimeters operate differently. Transverse polarisation is determined by measuring the vertical, up-down, asymmetry of the back-scattered photons on the TPOL calorimeter face, while longitudinal polarisation is determined by measuring the energy asymmetry in the LPOL calorimeter.

The TPOL calorimeter is separated horizontally into two halves. The energy sharing between the upper and lower halves is used to determine the impact position of the photon in the vertical direction. The up-down position asymmetry used to determine the polarisation relies on the conversion of the up-down energy asymmetry into a vertical position. This conversion is referred to as the ‘ $\eta - y$ transformation’. The dominant systematic errors in the polarisation measurement relate either to the linearity of the calorimeter energy response or to the precision with which the $\eta - y$ transformation is known. To determine the transformation precisely, in situ, during data-taking we have implemented a silicon-microstrip detector system. This system is composed of two $60 \times 60 \text{ mm}^2$ silicon-microstrip detectors placed in front of the calorimeter and behind a $1 X_0$ thick lead pre-radiator. The strip pitch of the detector measuring the vertical co-ordinate is $80 \mu\text{m}$. A detector with a strip pitch of $120 \mu\text{m}$ and for which every second strip is read out is used to measure the horizontal coordinate. A high flux of photons enter the TPOL detector. The energy deposited by these photons gives a dose of 5 Mrad per year over an area of only 0.1 mm^2 . In order to identify and correct for the effects of differential radiation damage in the silicon-microstrip detector a scintillating fibre mounted on a precision stage has been installed between the silicon-detector planes and the pre-radiator. The fibre will be scanned periodically across the face of the silicon detector in vertical steps of $2.5 \mu\text{m}$ and will allow differential radiation damage to be identified and corrected for. The upgraded TPOL detector has been commissioned using test beams at DESY and at CERN. The results demonstrate that the required performance has been achieved. The system has been installed, commissioned and is operating routinely in the HERA tunnel. A second iteration of front-end silicon-detector boards are currently being prepared for testing at Imperial College. These boards will be installed in the TPOL during the HERA shutdown in March 2003.

6 Physics analyses

During 2002 sixteen ZEUS physics papers were published or submitted for publication in various journals. In this section, we concentrate on those physics areas where the UK members of ZEUS have been particularly active.

6.1 Inclusive DIS cross-sections and structure function measurements

6.1.1 High Q^2 NC and CC scattering

ZEUS UK physicists are active and taking leading roles in all areas of ZEUS structure function and high Q^2 NC/CC cross-section extraction and analysis. The high- Q^2 e^-p NC and CC cross-

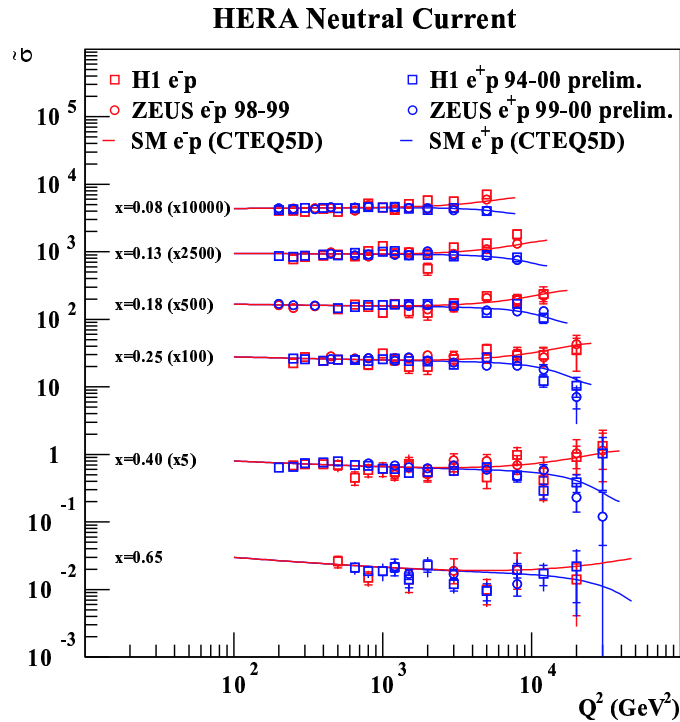


Figure 3: The reduced cross-sections for e^-p and e^+p NC scattering as a function of Q^2 at fixed x .

section measurements from 1998/99 running referred to in last year's report have both been submitted for publication [1, 2]. The analyses of the final samples of high- Q^2 NC and CC e^+p data taken before the shutdown for the HERA upgrade are in the final stages of preparation for publication. A couple of plots from the ICHEP02 Conference show the overall quality of the HERA-I data on high- Q^2 NC and CC cross-sections. The reduced cross section $\tilde{\sigma}_{\text{NC}}^{e^\pm p}$, where

$$\tilde{\sigma}_{\text{NC}}^{e^\pm p} = \frac{1}{Y_+} \frac{xQ^4}{2\pi\alpha^2} \frac{d^2\sigma_{\text{NC}}^{e^\pm p}}{dx dQ^2}, \quad (1)$$

is shown at fixed x as a function of Q^2 in figure 3. For Q^2 values above 1000 GeV^2 the e^-p cross section lies above the e^+p cross section; consistent with the SM expectation. The double differential CC cross section may be written as

$$\frac{d^2\sigma^{CC}}{dx dQ^2} = \frac{G_F^2}{2\pi x} \left(\frac{M_W^2}{M_W^2 + Q^2} \right)^2 \tilde{\sigma}_{\text{CC}}^{e^\pm p} \quad (2)$$

where the e^-p reduced cross section, $\tilde{\sigma}_{CC}^{e^\pm p}$, is given at leading order in QCD by

$$\tilde{\sigma} = u + c + (1 - y)^2(\bar{d} + \bar{s}) \quad (3)$$

(for e^+p , change quarks to anti-quarks and vice versa). The reduced cross sections, for both e^-p

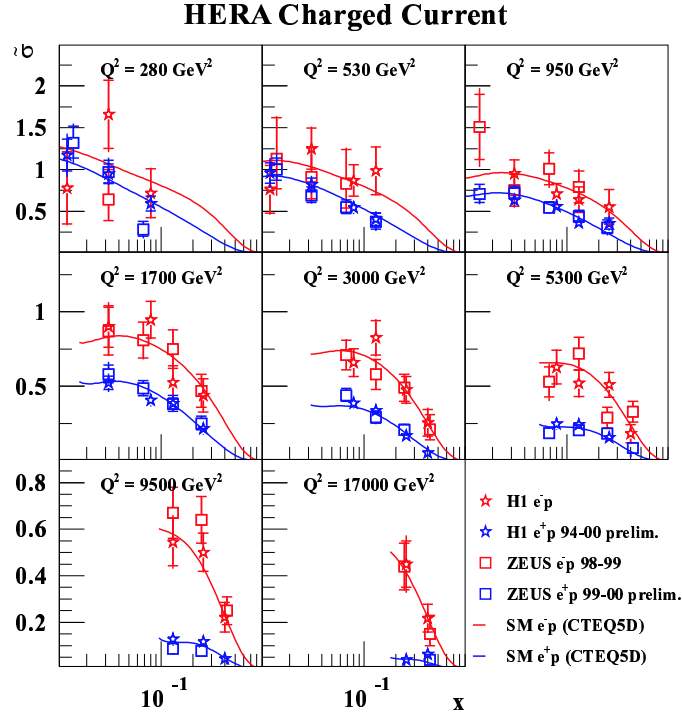


Figure 4: The reduced cross-sections for e^-p and e^+p CC scattering as functions of x at fixed Q^2 .

and e^+p , are plotted as functions of x at several fixed values of Q^2 in figure 4. The Standard Model, evaluated with the CTEQ5D PDFs, gives a good description of the data.

6.1.2 F_2 from Radiative Events

UK physicists have lead an analysis of deep inelastic scattering events with hard initial state radiation [3]. As the centre-of-mass energy of the subsequent ep interaction is decreased (as oppose to the fixed vaule for events without radiation), this allows the possibility of a direct measurement of the longitudinal structure function, F_L . The analysis is rather tricky because of a large background from ep bremsstrahlung events that has to be calibrated and subtracted statistically. As a first step towards an F_L measurement the ISR data from 3.8 pb^{-1} has been used to measure F_2 in the ranges $0.2 < Q^2 < 28.8 \text{ GeV}^2$, $8 \times 10^{-6} < x < 0.11$, which covers the region between ZEUS high precision measurements at very low Q^2 [4] and large luminosity data for Q^2 between 3 and 30000 GeV^2 [5]. Fig. 5 shows the ISR F_2 data together with earlier measurements and the QCD fit referred to in the next section.

6.1.3 NLO QCD fits

The UK has played a leading role in the interpretation of the data on the proton structure functions by performing NLO QCD fits, using the DGLAP formalism, to determine the parton density functions (PDFs) and α_S [6]. In the standard (ZEUS-S) fit, the high precision data on neutral current e^+p scattering [5] are fitted together with fixed-target data.

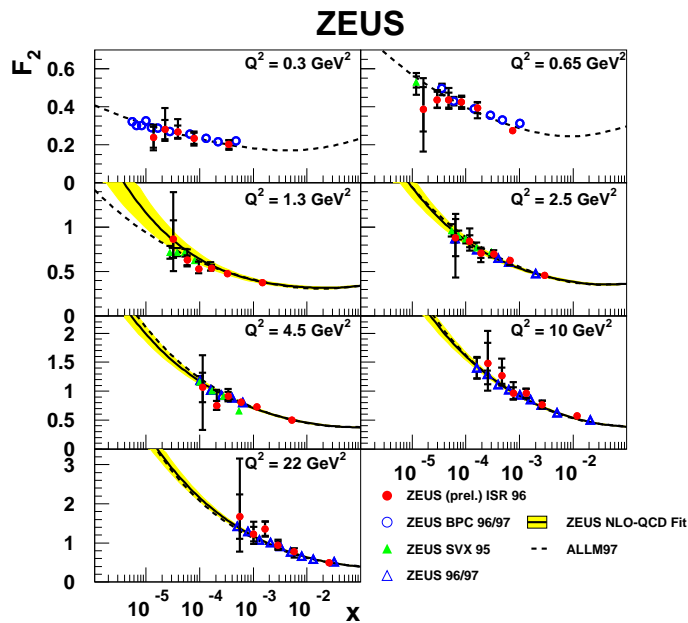


Figure 5: F_2 from ISR data as a function of x at fixed Q^2 .

A particular focus of this work has been the determination of the uncertainties on the parton distributions resulting from experimental sources. The ZEUS data are crucial for the determination of the gluon and the sea PDFs. These distributions are shown in Fig 6. The error bands shown take full account of correlated experimental systematic uncertainties from all contributing data sets, including their normalisation uncertainties. In this figure the additional uncertainty on these PDFs due to variation of the strong coupling constant $\alpha_s(M_Z)$ is shown. This can be accounted for with full correlations to the PDF parameters by allowing $\alpha_s(M_Z)$ to be a parameter of the fit (ZEUS- α_s fit). The ZEUS- α_s fit also determines the value of $\alpha_s(M_Z)$, leading to

$$\alpha_s = 0.1166 \pm 0.0008(\text{uncorr}) \pm 0.0032(\text{corr}) \pm 0.0036(\text{norm}) \pm 0.0018(\text{model}),$$

where the four uncertainties arise from the following: statistical and other uncorrelated sources; correlated systematic sources from all contributing experiments excluding their normalisation uncertainties; normalisation uncertainties; model uncertainty. The model uncertainty arises from variation of model inputs such as the value of Q_0^2 at which the input PDFs are parametrised, the form of the input parametrisation, the choice of data sets entering the fit and the kinematic cuts applied to these data sets, and the choice of heavy quark production scheme. The PDF parameters are less sensitive to the model assumptions than $\alpha_s(M_Z)$, thus it is clear that, *within the theoretical framework of leading twist NLO QCD*, the uncertainties due to model assumptions are not significant compared to the experimental uncertainties.

The NLO DGLAP formalism is expected to fail at low Q^2 . The combination of the new precise fit analysis and the precise low Q^2 data [4] make it possible to quantify this expectation. In Fig 7 the ZEUS-S fit is shown extrapolated back into the kinematic region of the ZEUS BPT 1997 data. It is clear that the formalism is unable to describe the data for $Q^2 \lesssim 1 \text{ GeV}^2$.

In the ZEUS-S fit, the valence PDFs are determined by the fixed target data, which suffer from uncertainties due to the need for heavy target corrections. However, a fit can be made to ZEUS data alone (ZEUS-O fit), if the high Q^2 e^+p data on the CC cross-section [7] and the

ZEUS

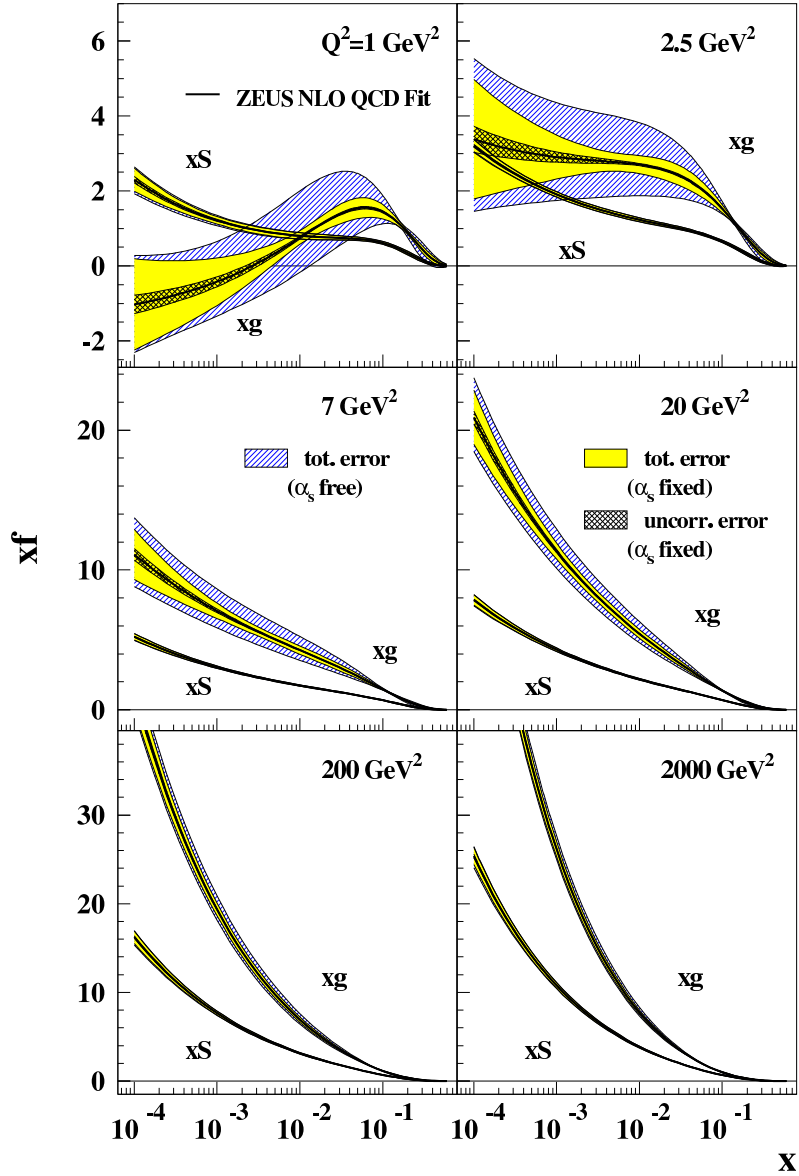


Figure 6: Comparison of gluon and sea distributions from the ZEUS-S NLO QCD fit for various Q^2 . The cross-hatched error bands show statistical and other uncorrelated systematic uncertainty, the grey error bands show the total experimental uncertainty including correlated systematic uncertainties and the hatched error bands show the additional uncertainty coming from variation of the strong coupling constant, $\alpha_s(M_Z)$.

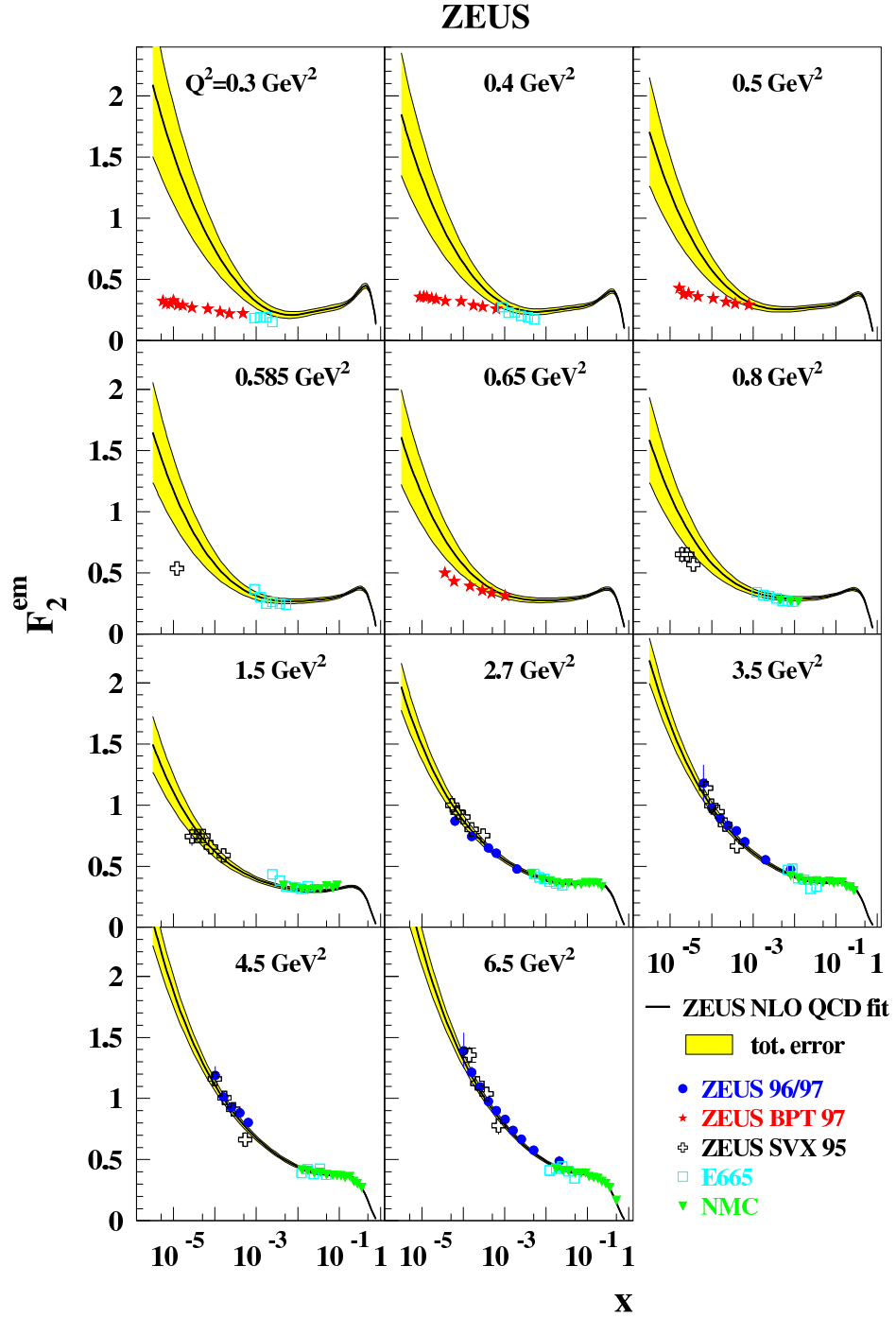


Figure 7: F_2 data at very low Q^2 compared to the backward extrapolated ZEUS-S NLO QCD fit. The error bands represent the total experimental error from both correlated and uncorrelated sources.

e^-p data on the CC [1] and NC [2] cross-sections are included. When this ZEUS-O fit is done using only the published e^+p data, the level of precision with which the valence distributions can be measured is approximately half of that of the ZEUS-S fit. However, if the e^+p data from 99/00 [8] are also included, then the level of precision is considerably improved. It is clear that the forthcoming high-luminosity running will allow us to significantly extend these studies.

6.2 Heavy quark production

ZEUS UK groups have been involved in many aspects of the programme to understand heavy quark production. Analyses investigating the production rate and nature of beauty and charm quarks are making significant contributions in a field which is still poorly understood. The production of charm quarks in DIS and accompanied by jets in photoproduction are now being measured precisely. This is discussed below along with the first measurement of open beauty production at ZEUS.

6.2.1 Charm production in DIS

Heavy quarks, particularly charm, are produced copiously in DIS, predominantly via the boson-gluon fusion (BGF) process. This means that measurements of charm production allow, in principle, a direct determination of the gluon density in the proton. Charm has traditionally been identified by two decay chains, $D^{*+} \rightarrow D^0\pi^+$, $D^0 \rightarrow K^-\pi^+$ or $D^0 \rightarrow K^-\pi^-\pi^+\pi^+$ which have low backgrounds but also have small branching ratios. Using a luminosity of 37 pb^{-1} , ZEUS has published a measurement of charm production via these two decay channels [9]. Predictions of NLO QCD describe the data well over the full range in Q^2 . The gluon distribution in the proton used was determined from fits to inclusive measurements of the proton structure function, F_2^p . The consistency of this prediction with the charm data demonstrates the universality of the gluon distribution in the proton, independent of the final state. Using all currently available ZEUS data along with other decay channels will greatly improve the precision of these measurements. UK physicists are taking a leading rôle in both of these directions. Very high-statistics measurements of heavy quark production in DIS will be a major goal with the new data to come with the upgraded HERA accelerator and ZEUS experiment.

6.2.2 Charm production in diffraction

Charm production is a key process for investigating the dynamics of diffractive DIS, since the charm-quark mass provides a hard scale and charm production is known to be sensitive to gluon-exchange process in DIS generally. In a recent ZEUS analysis [10], carried out by ZEUS UK physicists, two contrasting theoretical approaches were compared with the data. In “resolved-pomeron models”, charm is produced via BGF in which an exchanged Pomeron has a partonic structure. The other models, “two gluon exchange”, are based on the virtual photon decomposing into $q\bar{q}$ and $q\bar{q}g$ states which then interact with the proton; the simplest form is the exchange of two gluons.

In Fig. 8, measurements of diffractive D^* production in DIS for various kinematic variables are shown using an integrated luminosity of 44 pb^{-1} . The general methods of reconstruction of both the D^* and DIS kinematics were the same as for the inclusive measurement in the previous section. The experimental signature for diffractive production is a large rapidity gap between the scattered proton and the hadronic system, X , from the dissociated virtual photon. A cut on the most forward energy deposit of $\eta_{\text{max}} < 2$ was made to select diffractive events. In Fig. 8, the resolved pomeron model, ACTW, and the two gluon exchange model, SATRAP, give a similar description of the data. Another two gluon exchange model, BJLW, gives the best description

ZEUS

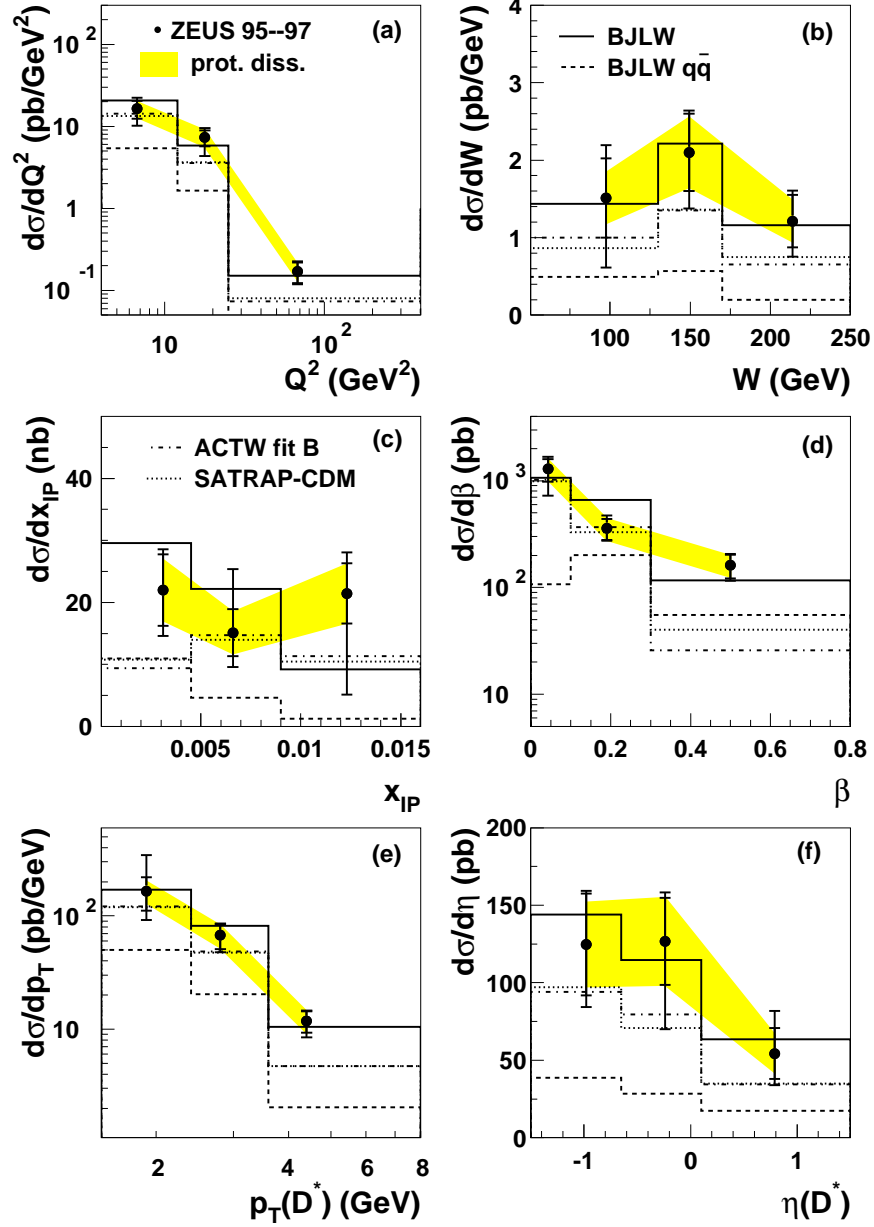


Figure 8: Differential cross sections for $D^{*\pm}$ diffractive production in DIS. The cross sections are shown as a function of a) Q^2 , b) W , c) x_P , d) β , e) $p_T(D^*)$ and f) $\eta(D^*)$.

of the data, particularly for the distribution in β which in a resolved-pomeron model can be interpreted as the fraction of the pomeron's momentum carried by the struck parton.

6.2.3 Charm production with jets

With the larger statistical sample in the photoproduction regime ($Q^2 < 1 \text{ GeV}^2$), charm production accompanied by jets, is providing a detailed picture of many aspects of QCD and, in particular, the charm content of the photon. The first measurement of charm quarks inside jets was published in 1999 [11], with UK physicists as principal authors. The results showed for the first time that charm is produced copiously in resolved-photon events. Building on these results, resolved-photon processes have been studied further in order to understand if the charm quark is an active parton in the photon or produced only in the hard scatter.

6.2.4 Probing the hard subprocess

In charm events where two jets are produced, measurements of the angle, θ^* , between the jet-jet axis and beam direction in the dijet rest frame allow the dominant propagator in the hard scatter to be determined. In contrast to measurements of inclusive dijet production, the absolute value of $\cos\theta^*$ could be determined since the two jets can be distinguished; the jet associated with the D^* was defined with respect to the proton direction. Events in which the photon acts as a pointlike object (BGF) have a quark propagator; the cross section as a function of $\cos\theta^*$ is symmetric and $\propto (1 - |\cos\theta^*|)^{-1}$. If charm were not active in the photon, then charm in resolved-photon processes would be produced only via gluon-gluon fusion which has a quark as the propagator and has a distribution similar to that of BGF.

Events enriched in direct- or resolved-photon processes can be selected by requiring $x_\gamma^{OBS} > 0.75$ and $x_\gamma^{OBS} < 0.75$, respectively; the variable x_γ^{OBS} is the fraction of the photon's momentum taking part in the production of the two jets of highest transverse energy. Figure 9 shows the measured $\cos\theta^*$ distribution in the two regions of x_γ^{OBS} . The measurement is based on a luminosity 119 pb^{-1} , almost all of the available pre-upgrade data. For $x_\gamma^{OBS} > 0.75$, the data show a shallow rise consistent with events having a quark propagator, whereas for $x_\gamma^{OBS} < 0.75$, the data show a shallow rise to positive $\cos\theta^*$ and a more rapid rise to negative $\cos\theta^*$. This is consistent with the dominance of a gluon propagator which has a cross section which is $\propto (1 - |\cos\theta^*|)^{-2}$. Resolved-photon events with a gluon propagator can only arise if the charm is active in the photon ($Q_\gamma g_P \rightarrow Qg$). The data is adequately described by predictions from the PYTHIA MC simulation and provides the strongest evidence so far of a heavy quark density in the photon.

6.2.5 The charm fragmentation function

In contrast to the the production of charm quarks which is described by pQCD, their subsequent hadronisation into mesons is described by phenomenological models. Fragmentation functions are used to parameterise the transfer of the quark's energy to a given meson; the transition from a charm quark to a D^* meson is the subject of this section. Many forms of fragmentation functions exist with tunable parameters which are fixed from fits to data, usually from experiments at e^+e^- colliders. The form of the fragmentation has not been measured for D^* mesons at HERA or at $p\bar{p}$ colliders. A measurement of the fragmentation function at HERA and its comparison with data from experiments at e^+e^- colliders provides a test of the universality of charm fragmentation. The available data from e^+e^- experiments is not very precise. Therefore the fitted fragmentation function remains a significant source of uncertainty in calculations of hadron-hadron or electron-proton cross sections for the production of D^* mesons.

ZEUS

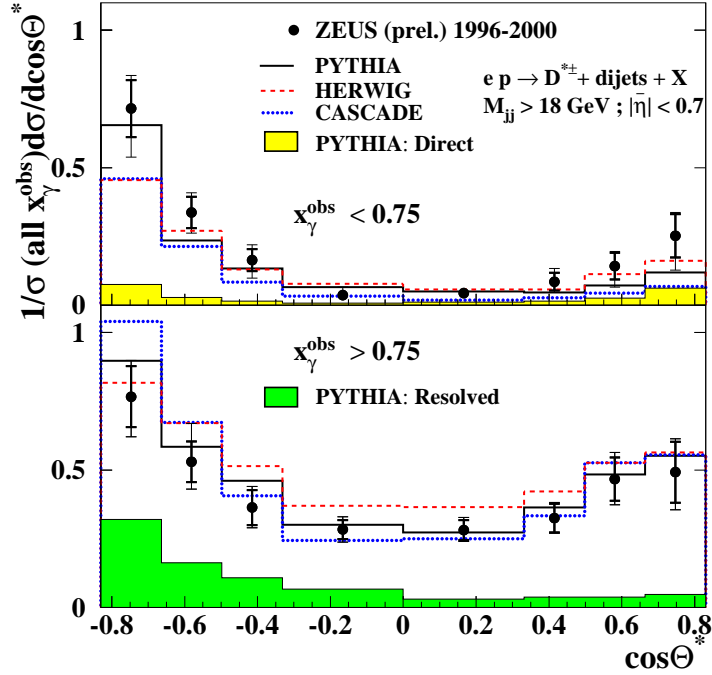


Figure 9: The $\cos\theta^*$ distribution in charm-tagged events for $x_\gamma^{OBS} > 0.75$ and $x_\gamma^{OBS} < 0.75$. Predictions from the PYTHIA MC are compared to the data.

A parameterisation often used to describe the fragmentation of heavy quarks is the Peterson function, which has the form $f(z) \propto 1/[z(1 - 1/z - \epsilon/(1 - z))^2]$, where ϵ is a free parameter. The fragmentation variable, z , is calculated as $z = (E + p_{\parallel})^{D^*}/(E + p_{\parallel})^{\text{jet}}$, where p_{\parallel} is the longitudinal momentum of the D^* meson relative to the axis of the associated jet of energy, E^{jet} . This function and the option to vary ϵ is available within the PYTHIA MC simulation. The value of ϵ was varied in the range 0.01 to 0.1, with the Lund string fragmentation model used for lighter flavours. For each value in the MC simulation, the full event record was generated and the kinematic requirements applied, allowing a direct comparison with the data. The result of varying ϵ is shown in Fig. 10. Here it can be seen that values as low as $\epsilon = 0.02$ are disfavoured, producing a much harder spectrum than the data, while values as high as $\epsilon = 0.1$ results in too soft a spectrum and are therefore also disfavoured. The MC was fit to the data via a χ^2 -minimisation procedure to determine the best value of ϵ . The result of the fit is $\epsilon = 0.064 \pm 0.006_{-0.008}^{+0.011}$, which is somewhat larger than the default value used in PYTHIA of 0.05. This value was then input into the MC and the result compared in Fig. 10; the data are well described.

The data has been qualitatively compared with the results from e^+e^- experiments; the general features of the data are the same. A more quantitative comparison of the data shown and hence a test of universal charm fragmentation can only be made by simultaneously fitting the data within a given model, such as the Peterson fragmentation within the framework of the PYTHIA simulation. This fragmentation function can then be implemented into a given calculation to improve the precision of future calculations to be compared with charm production at HERA.

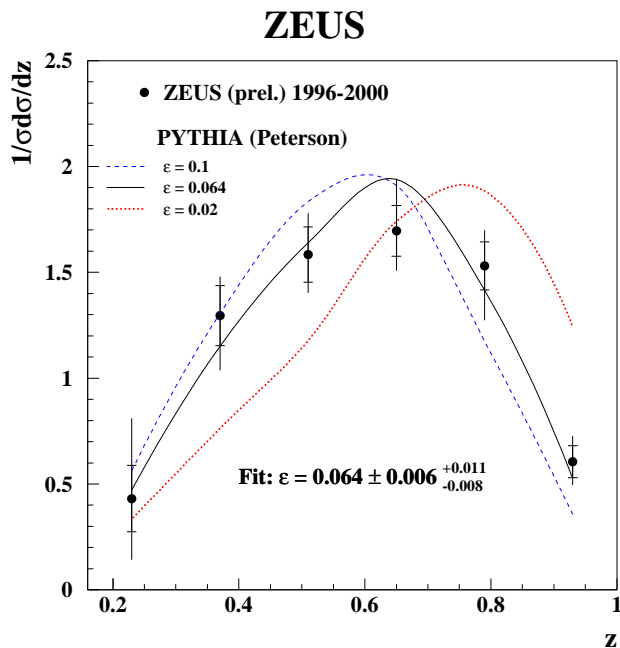


Figure 10: $1/\sigma(d\sigma/dz)$ for D^* production, where $z = (E + p_{\parallel})^{D^*} / (E + p_{\parallel})^{\text{jet}}$. Data (points) are compared with PYTHIA MC predictions for values of the parameter $\epsilon = 0.1$ (dashed line), $\epsilon = 0.064$ (solid line) and $\epsilon = 0.02$ (dotted line), in the Peterson fragmentation function.

6.2.6 Beauty production

Heavy quarks can also be detected by identifying electrons from their decay. This is done by measuring the distinctive rate of energy loss of electrons in the CTD, as well as the way they interact in the calorimeter. Results by UK physicists using this method show a significant production rate for beauty quarks. Existing measurements of open beauty production from HERA, $\gamma\gamma$ collisions at LEP and $p\bar{p}$ colliders show cross sections that are high when compared to standard NLO QCD predictions. A direct comparison of the ZEUS result with an NLO QCD prediction is also possible by using a Monte Carlo to extrapolate to the $b\bar{b}$ cross section in a limited kinematic region. This extrapolated cross section also lies above the theoretical prediction [12].

Understanding such results is an important test of QCD and a necessary step towards understanding the new physics potential of future colliders. The results also represent a substantial technical triumph in the operation and understanding of the CTD dE/dx readout, a UK responsibility from the beginning of ZEUS.

The presence of heavy quarks in the evolution of the photon structure offers a promising window for understanding the development of QCD structure, splitting functions and threshold effects. The ability at HERA to select concurrently on jet transverse energy, E_T^{jet} , photon virtuality and x_γ^{OBS} , as well as to compare heavy flavour jets with untagged jets, makes it uniquely suitable for detailed studies in this area. Thus heavy flavour jet production will be a growth area, and is a major driving force behind the UK's involvement in the MVD. The GTT will play a vital part in allowing these events to be saved at relatively low E_T^{jet} even after the upgrade, particularly if charm enrichment can be implemented.

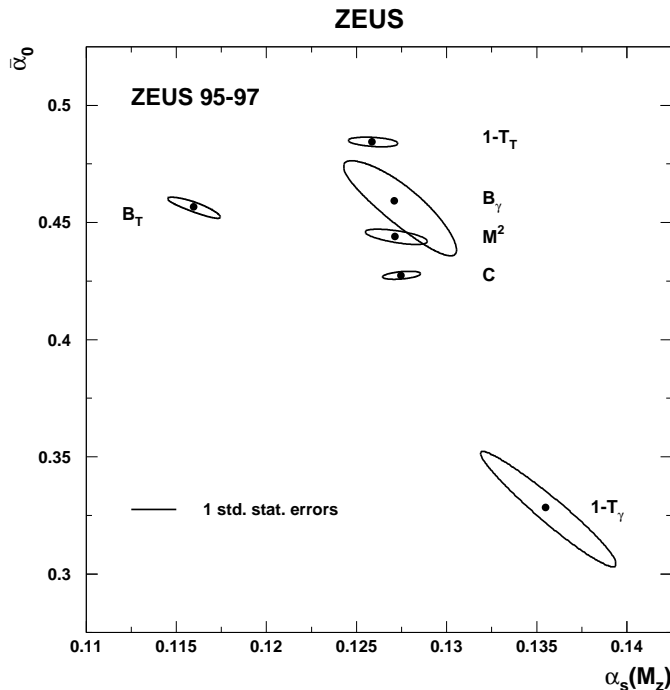


Figure 11: Contour plots for $\alpha_s(M_Z)$ and $\bar{\alpha}_0$ fitted to the mean values of the event-shape variables. The fits are based on DISASTER++. One standard deviation contours are shown, determined using statistical uncertainties only.

6.3 QCD and the hadronic final state

6.3.1 Event Shapes

A recent revival of interest in the study of event shape measurements has been prompted by theoretical developments in the understanding of hadronisation or power corrections. Power corrections allow perturbative QCD (pQCD) calculations to be extended into the region of low momentum transfers using approximations to higher-order graphs. At HERA, the Q^2 scale can be varied over four orders of magnitude enabling power corrections (proportional to $1/Q^n$) to be studied in detail. The data are compared to theoretical expectations for the power corrections and the effective coupling $\alpha_0(\mu_I)$, specified at the infra-red matching scale $\mu_I = 2$ GeV, and $\alpha_s(M_Z)$ are extracted. The event-shapes studied were thrusts (T), jet broadening (B), the invariant jet mass (M) and the C-parameter. The variables are calculated in the current region of the Breit frame. The thrust and broadening are calculated with respect to two longitudinal axes: the virtual photon direction (denoted by the subscript γ) and the axis that maximises the thrust (denoted by the subscript T .)

Using NLO calculations plus the power correction approach, the mean event shape values versus Q are measured. Overall, a reasonable description of the data can be achieved, although the x -dependence of variables T_γ and B_γ is not well described. The major theoretical uncertainty is that due to the renormalisation scale. The results of two-parameter fits to the ZEUS data both including and excluding the data at low- x are shown in Fig. 11 [13]. The correlation of $\alpha_0(\mu_I)$ and $\alpha_s(M_Z)$ is high and negative for $\langle T \rangle$ but is less significant for other event shape variables. In each case, the data for the means of B_γ , $1 - T_T$, C and M^2 are described reasonably well by the theory with values of the universal non-perturbative parameter $\alpha_0(\mu_I) \approx 0.45$ and $\alpha_s(M_Z) \approx 0.127$. There are, however, theoretical uncertainties due to uncalculated higher-order

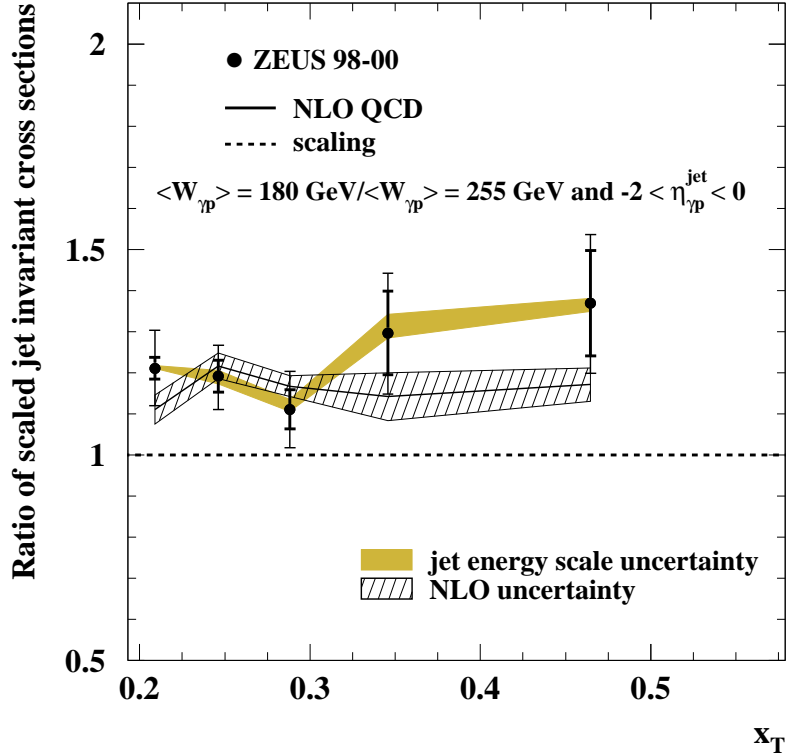


Figure 12: Measured ratio of scaled jet invariant cross sections, after correcting for the difference in the photon flux between the two $W_{\gamma p}$ intervals, as a function of x_T (dots). The dashed line is the scaling expectation.

x -dependent terms which appear to be especially significant for B . Ongoing refinements will generate further insight into non-perturbative QCD mechanisms in the generation of hadronic final states at high energies.

6.3.2 Scaling Violations in γP Interactions

Jet production provides a testing ground for the theory of the strong interaction between quarks and gluons. This analysis concentrates on the comparison of jet cross sections for the same reaction at different centre-of-mass energies. This highlights the effects of scaling violations, while a QCD analysis of jet-production rates allows the measurement of the strong coupling constant, α_s .

Inclusive jet cross sections have been measured as a function of the jet transverse energy (E_T^{jet}) in the range $E_T^{\text{jet}} > 17$ GeV for jets with a pseudorapidity $-1 < \eta^{\text{jet}} < 2.5$ and a γP centre-of-mass energy in the range $142 < W_{\gamma P} < 293$ GeV. Scaled invariant cross sections have been measured as a function of the dimensionless variable $x_T = 2E_T^{\text{jet}}/W_{\gamma P}$ in the range $0.150 < x_T < 0.654$ for two $W_{\gamma P}$ values (180 and 255 GeV.) Next-to-leading-order QCD calculations give a reasonable description of the measured differential cross sections in magnitude and shape. Figure 12 shows the ratio of scaled invariant cross sections at two $W_{\gamma P}$ values shows clear non-scaling behaviour. A value for the strong coupling constant of $\alpha_s(M_Z) = 0.1224 \pm 0.0001(\text{stat.})_{-0.0019}^{+0.0022}(\text{exp.})_{-0.0042}^{+0.0054}(\text{th.})$ has been extracted from a QCD analysis of the measured $d\sigma/dE_T^{\text{jet}}$. The variation of α_s with E_T^{jet} is in good agreement with the running of α_s as predicted by QCD.

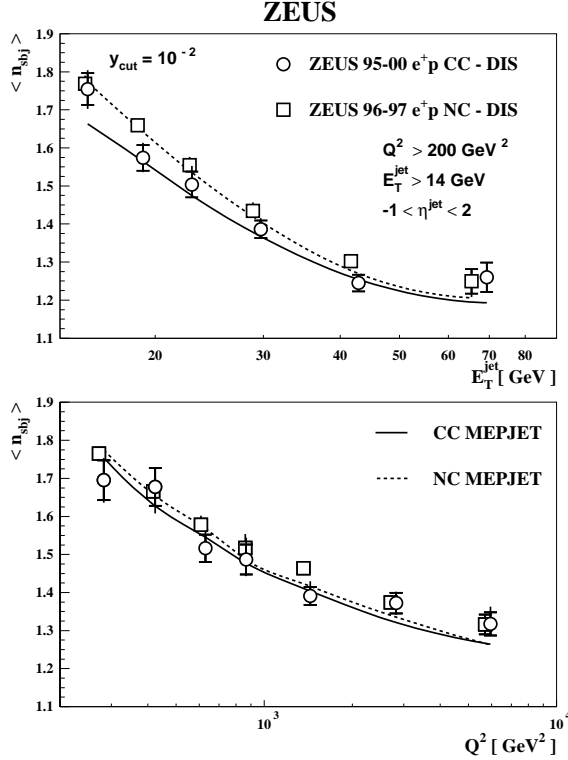


Figure 13: Mean subjet multiplicity, $\langle n_{sbj} \rangle$, at $y_{cut} = 10^{-2}$ as a function E_T^{jet} , (top) and Q^2 (bottom) for inclusive jet production with $E_T^{jet} > 14 \text{ GeV}$ and $-1 < \eta^{jet} < 2$. The NLO QCD predictions obtained with MEPJET using the CTEQ4 sets of proton PDFs are shown.

6.3.3 Jet Production in Charge Current Events

Jet production in charged-current (CC) DIS provides a testing ground for QCD as well as for the electroweak sector of the Standard Model (SM). In addition, searches for new physics rely crucially on accurate determinations of event rates and cross sections from SM processes. Up to leading order in the strong coupling constant α_s , jet production in CC DIS proceeds via the quark-parton model ($Wq \rightarrow q$), the QCD-Compton ($Wq \rightarrow qg$) and W -gluon fusion ($Wg \rightarrow qq$) processes.

The production rates as well as the substructure of jets have been studied in charged current deep inelastic e^+p scattering for $Q^2 > 200 \text{ GeV}^2$ using an integrated luminosity of 110.5 pb^{-1} . The differential inclusive jet cross sections were measured in the kinematic region defined by $Q^2 > 200 \text{ GeV}^2$ and $y < 0.9$. These cross sections include every jet of hadrons in the event with $E_T^{jet} > 14 \text{ GeV}$ and $-1 < \eta_{jet} < 2$. The $d\sigma/d\eta^{jet}$ distribution has a maximum at $\eta^{jet} \sim 1$. Both the ARIADNE Monte Carlo generator prediction and the NLO QCD calculations give a reasonable representation of the data, although ARIADNE gives a better description of the data.

The dijet differential inclusive jet cross sections were measured in the same kinematic region of Q^2 and y . These cross sections refer to the two jets of hadrons with highest transverse energy in the event with $E_T^{jet,1} > 14 \text{ GeV}$, $E_T^{jet,2} > 5 \text{ GeV}$ and $-1 < \eta^{jet} < 2$; $E_T^{jet,1}$ ($E_T^{jet,2}$) is the transverse energy of the jet with the highest (second highest) transverse energy in the event. Again, the NLO QCD calculations give a reasonable representation of the data.

The mean subjet multiplicity, $\langle n_{sbj} \rangle$, was determined using the inclusive sample of jets in the same kinematic region and compared to the jets in neutral current events. The measurements of $\langle n_{sbj} \rangle$ at $y_{cut} = 10^{-2}$ as a function of E_T^{jet} in CC and NC DIS are compared in Fig. 13 (top). The $\langle n_{sbj} \rangle$ is slightly larger for jets in NC DIS than for CC DIS for a given jet transverse energy.

The NLO QCD predictions show the same behaviour as that observed in the data. The subject multiplicities were also examined as a function of Q^2 in CC and NC DIS (Fig. 13 bottom). The values of $\langle n_{sbj} \rangle$ in CC and NC DIS are similar and are in agreement with the NLO predictions. Hence, the differences observed in the subject multiplicity as function of E_T^{jet} can be attributed to the differences in the Q^2 spectrum of the two processes.

A fit of the measured $\langle n_{sbj} \rangle$ as a function of E_T^{jet} at $y_{\text{cut}} = 10^{-2}$ provides a determination of the strong coupling constant. The value of $\alpha_s(M_Z)$ determined by fitting the NLO QCD calculations to the measured $\langle n_{sbj} \rangle$ for $E_T^{\text{jet}} > 25$ GeV is

$$\alpha_s(M_Z) = 0.1202 \pm 0.0052(\text{stat})_{-0.0019}^{+0.0060}(\text{syst.})_{-0.0053}^{+0.0065}(\text{th.}).$$

This result is consistent with other recent ZEUS determinations and with the PDG value.

6.3.4 Virtual-photon structure

It has been long established that the real photon, $Q^2 = 0$, has a partonic structure, while at high Q^2 it is commonly considered to be a point-like particle and used as a probe of the partonic structure of hadronic targets. Even though considerable progress from the theoretical and experimental sides has recently been made in investigating the structure of virtual photons, the PDFs of the virtual photon are less well known than those of the real photon.

The differential dijet cross section, $d\sigma/dQ^2$, for $E_T^{\text{jet},1} > 7.5$ GeV, $E_T^{\text{jet},2} > 6.5$ GeV, $-3 < \eta^{\text{jet}} < 0$ and $0.2 < y < 0.55$ in the range $0.1 < Q^2 < 2000\text{GeV}^2$ for the direct-enhanced region ($x_\gamma^{\text{obs}} > 0.75$) and the resolved-enhanced region ($x_\gamma^{\text{obs}} < 0.75$), together with the total dijet cross section have been measured. The measurements are precise and cover a wide range of photon virtualities, including the transition region from photoproduction to DIS. The measured cross sections fall by more than four orders of magnitude over this Q^2 range. The cross section for $x_\gamma^{\text{obs}} < 0.75$ falls more rapidly than that for $x_\gamma^{\text{obs}} > 0.75$. Even though the total cross section is dominated by interactions with ($x_\gamma^{\text{obs}} > 0.75$) for $Q^2 \geq 10$ GeV², there is still a contribution of about 24% from low- x_γ^{obs} events even for Q^2 as high as 500 GeV².

The Q^2 dependence of the direct- and resolved-enhanced components of the dijet cross section has been studied in more detail using the ratio

$$R = \frac{d\sigma}{dQ^2(x_\gamma^{\text{obs}} < 0.75)} / \frac{d\sigma}{dQ^2(x_\gamma^{\text{obs}} > 0.75)}.$$

The experimental and theoretical uncertainties largely cancel in the ratio, so that a more stringent test of the theory is possible. Figure 14 shows the ratio R as a function of Q^2 in three different regions of $\overline{E_T^2}$. The Q^2 dependence of the data is stronger at low $\overline{E_T^2}$, where the photon is expected to have structure, than for higher $\overline{E_T^2}$, showing that the resolved contribution is indeed suppressed at low Q^2 as $\overline{E_T^2}$ increases. The NLO predictions fail to describe the Q^2 dependence of R : the calculations significantly underestimate the measured ratio for $Q^2 < \overline{E_T^2}$. This disagreement between the data and the NLO calculations decreases as $\overline{E_T^2}$ increases, but, at the highest Q^2 and $\overline{E_T^2}$ the theory still falls below the data. Even though the JetVip NLO program includes the Q^2 -dependent structure of the photon, it describes the data less well at low Q^2 than does DISASTER++ in all $\overline{E_T^2}$ regions. This is due to the fact that the $x_\gamma^{\text{obs}} < 0.75$ contribution is lower and the $x_\gamma^{\text{obs}} > 0.75$ is higher than in DISASTER++.

6.3.5 Rapidity Gap between Jets in Photoproduction

Events produced in hadronic collisions with two jets of high transverse energy separated by a large rapidity gap containing little or no energy provide an ideal environment to study the

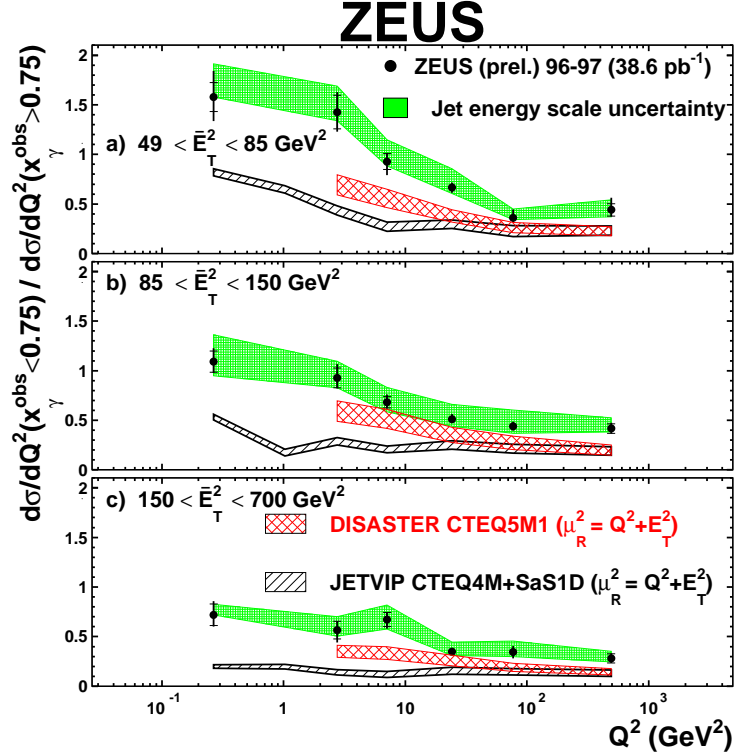


Figure 14: Measured ratio R as a function of Q^2 in different regions of E_T^2 (black dots). The NLO QCD calculations of JetVip and DISASTER++ are also shown.

mechanism of colour-singlet exchange in a regime where perturbative QCD should be applicable. The dominant production mechanism for such events is a hard interaction between partons from the incoming hadrons interacting via a quark or gluon propagator. This exchange of colour quantum numbers gives final state jets that are colour connected both to each other and to the hadronic remnants. This leads to energy flow that populates the pseudorapidity region both between the hadronic remnants and between the jets themselves. Events with a large rapidity gap between the jets would then be a signature for the exchange of a colour singlet. This exchanged object could be either an electroweak boson, or some strongly-interacting Pomeron-like object. The high transverse energy provides a perturbative hard scale at each end of the colour-singlet exchange, so that the cross section should be fully calculable in perturbative QCD.

The data fall for increasing rapidity gap, but levels out as the size of the gap increases. The predictions of Pythia and Herwig without colour-singlet exchange show an approximately exponential dependence on the size of the rapidity gap, consistent with the purely statistical behaviour seen in studies of rapidity gaps in e^+e^- annihilation. The predictions lie below the data for larger rapidity gap values. In particular, the Pythia prediction is significantly lower than that from Herwig without colour-singlet exchange. Herwig is known to be able to produce a high rate of rapidity-gap events in inclusive DIS processes, without any explicit colour-singlet-exchange contribution, the inclusion of which improves the comparison with the present data, although the model still lies below the data for larger rapidity gaps.

Figure 15 shows the gap fraction as a function of x_γ^{obs} . A significantly larger gap fraction is observed at high x_γ^{obs} . This may be due to the reduced probability of gluon radiation into the gap from the t-channel quark propagator in direct events. Neither of the Herwig models gives a good description at high x_γ^{obs} . At lower x_γ^{obs} , the model including colour singlet exchange shows larger gap fractions. However, both simulations are consistent with the data, except for the lowest jet transverse energy cut values, where the model without colour-singlet exchange gives a better

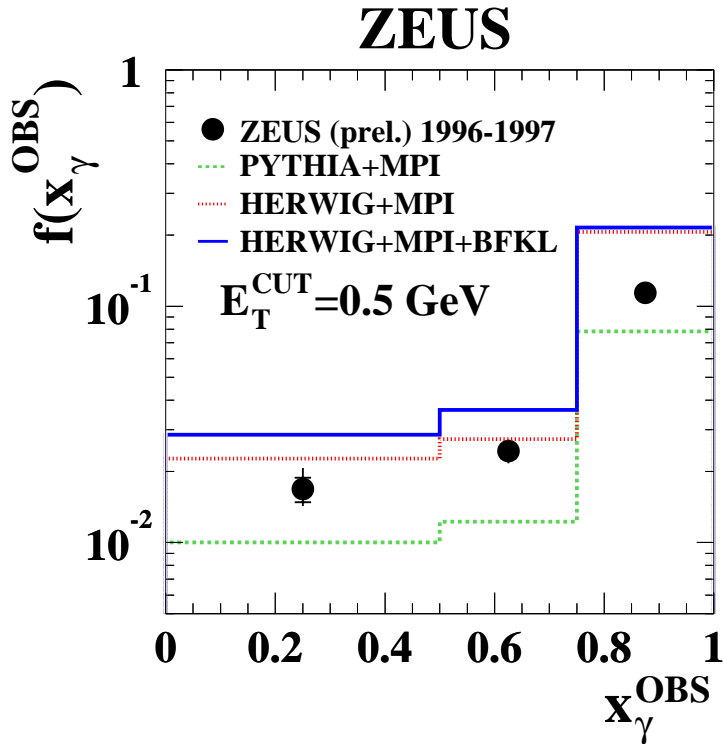


Figure 15: The gap fraction, f , as a function of x_γ^{OBS} . The data are shown as the solid points, where the inner error bar shows the statistical uncertainty and the outer error bar shows the statistical and systematic uncertainty added in quadrature.

agreement.

The excess of gap events with large rapidity gaps and low x_γ^{obs} with respect to the predictions without colour-singlet exchange suggests that this component may be required. However, the large differences between the models without explicit colour-singlet exchange and the poor description of the high x_γ^{obs} gap fraction by any of the models precludes any firm conclusions on the underlying dynamics.

6.3.6 Multijet Production in Photoproduction

The study of multijet production provides sensitive tests of pQCD at intrinsically higher order in the strong coupling constant. In resolved events, it is possible for further hard scatters to take place between the proton and photon remnants. This is known as multiple parton scattering, or multi-parton interactions.

Photoproduction events with three jets in the final state have been measured at HERA using variables defined in the scheme of Geer and Asakawa [14]. Four-jet observables defined under the same scheme have also been measured. These variables span the multijet parameter space and have a relatively simple interpretation within the context of pQCD. The variables are defined in the four-jet centre-of-mass frame. The two jets of lowest two-jet invariant mass were combined to form a single pseudo-jet system. The resulting three systems are labelled 3, 4 and 5 in order of decreasing energy and the resulting pseudo-three-jet system can be described by the following dimensionless variable:

$$\cos \theta_3 = \frac{p_3 \cdot p_{\text{beam}}}{|p_3| |p_{\text{beam}}|}$$

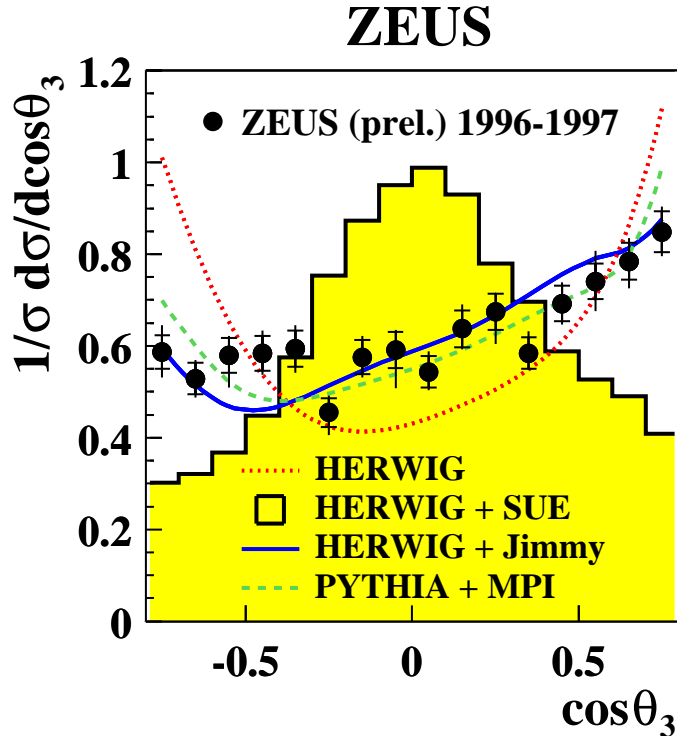


Figure 16: Figure 3: The $\cos \theta_3$ distribution for the inclusive sample. The ZEUS data are shown by the solid points. The inner error bars show the statistical uncertainty and the outer error bars show the statistical and systematic uncertainties combined in quadrature. The dotted line shows the prediction from the HERWIG Monte Carlo and the histogram shows the prediction after inclusion of the SUE model. The solid line shows HERWIG+Jimmy and the dashed line is the prediction of PYTHIA+MPI.

where p_{beam} is the average beam direction.

The $\cos \theta_3$ distribution shows a relatively flat distribution with an enhancement in the forward direction compared to the backward, Figure 16. This is suggestive of a large contribution from low- x_γ partons, which tend to be boosted further forward compared to those at high x_γ (for the same fraction of the proton momentum, x_p , entering the hard scatter). The HERWIG Monte Carlo with no simulation of the underlying event is unable to describe the distribution of the data. In particular, this model shows a relatively symmetric distribution enhanced in both the forward and backward directions. The data do not indicate such a strong tendency for the highest-energy pseudo-jet to lie close to the beam. Including a simulation of a soft underlying event is disfavoured by the data in this kinematic region, as indicated by the HERWIG+SUE model. In contrast, inclusion of multi-parton interactions leads to a significantly improved description of the data. In particular, both the HERWIG+Jimmy and the PYTHIA+MPI models show a relatively flat distribution with an enhancement in the forward direction, in accordance with the general trend of the data.

6.4 Prompt photons in deep inelastic scattering

A first study of prompt photon production, with and without an accompanying jet, in deep inelastic scattering is nearing completion. The cross sections have been compared with some new NLO QCD calculations by Kramer and Spiesberger (Fig. 17). This is an area which could well benefit from higher integrated luminosities.

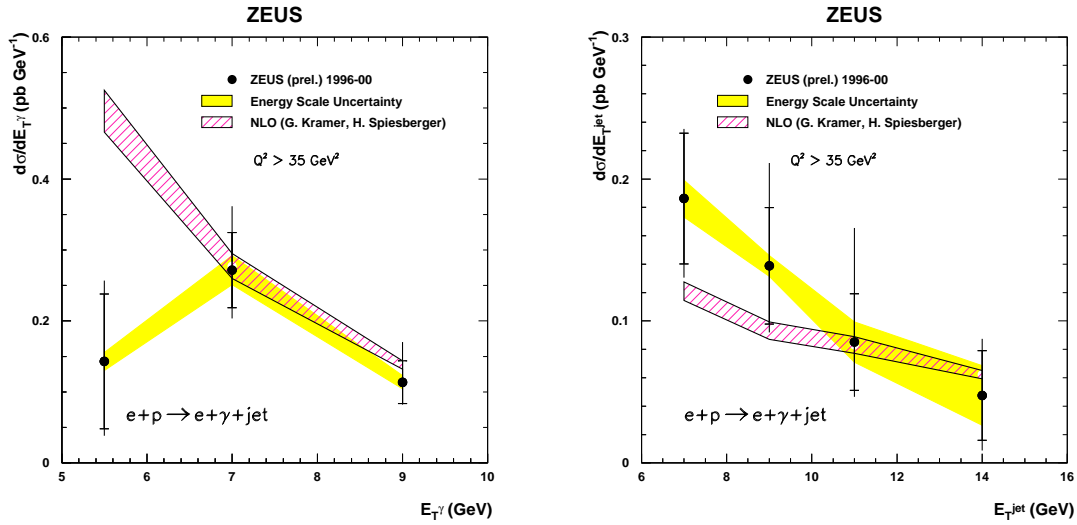


Figure 17: Prompt photon production in DIS $e + p \rightarrow e + \gamma + jet + X$. LH plot E_T^γ spectrum; RH plot E_T^{jet} spectrum.

6.5 Other Topics

Work on strange particle production (K_s and Λ in particular) mechanisms in high E_T photoproduction, reported last year continues [15].

Studies on production mechanisms for isolated high p_T leptons with large missing energy, where there is a long standing discrepancy between ZEUS and H1 are focusing on single top production and the possibility of extending this type of analysis to include high p_T jet final states as well.

References

- [1] ZEUS Collaboration, S. Chekanov et al., *Measurement of High- Q^2 Charged Current Cross Sections in e^-p Deep Inelastic Scattering at HERA*, DESY-02-064, Phys.Lett. **B539** (2002) 197-217.
- [2] ZEUS Collaboration, S. Chekanov et al., *Measurement of High- Q^2 Neutral Current Cross Sections in e^-p Deep Inelastic Scattering at HERA*, DESY-02-113, submitted to Eur.Phys.J
- [3] ZEUS Collaboration, *Measurement of the structure functions F_2 and F_L using initial state radiative events at HERA*, paper 771 submitted to ICHEP02, Amsterdam July 2002.
- [4] ZEUS Collaboration, J.Breitweg et al., *Measurement of the Proton Structure Function F_2 at Very Low Q^2 at HERA*
- [5] ZEUS Collaboration, S.Chekanov et al., *Measurement of the neutral current cross-section and F_2 structure function for deep inelastic e^+p scattering at HERA* Eur. Phys. J. **C21** (2001) 443. Phys. Lett. **B487** (2000) 53.
- [6] ZEUS Collaboration, S. Chekanov et al., *A ZEUS next-to-leading-order QCD analysis of data on deep inelastic scattering*, DESY-02-105, accepted by Phys.Rev.D
- [7] ZEUS Collaboration, J.Breitweg et al., *Measurement of High Q^2 Charged-Current e^+p Deep Inelastic Scattering Cross Sections at HERA* Eur. Phys. J. **C12** (2000) 411.

- [8] ZEUS Collaboration, S. Chekanov et al., *Measurements of High- Q^2 Neutral Current Cross-Sections in e^+p Deep Inelastic Scattering at HERA*, and *Measurements of High- Q^2 Charged Current Cross-Sections in e^+p Deep Inelastic Scattering at HERA* Abstracts 630 and 631, Submitted to Int. Conf. on High Energy Physics, July2001, Budapest.
- [9] ZEUS Collaboration, J. Breitweg et al., *Measurement of $D^{*\pm}$ production and the charm contribution to F_2 in deep inelastic scattering at HERA*, Eur. Phys. J. **C12** (2000) 35.
- [10] ZEUS Collaboration, S. Chekanov et al., *Measurement of diffractive production of $D^{*\pm}$ (2010) mesons in deep inelastic scattering at HERA.*, DESY 02-082, submitted to Phys. Lett. B.
- [11] ZEUS Collaboration, J. Breitweg et al., *Measurement of inclusive $D^{*\pm}$ and associated dijets cross sections in photoproduction at HERA*, Eur. Phys. J. **C6** (1999) 67.
- [12] ZEUS Collaboration, J. Breitweg et al., *Measurement of open beauty production in photoproduction at HERA*, Eur. Phys. J. **C18** (2001) 625
- [13] ZEUS Collaboration, S. Chekanov et al., *Measurement of event shapes in deep inelastic scattering at HERA*, DESY-02-198, to be published.
- [14] S. Geer and T. Asakawa, Phys. Rev. D53, 4793 (1996).
- [15] S. Boogert; *Strange Hadron Production*, 10th International Workshop on Deep Inelastic Scattering, May 2002, Cracow, Poland.

Appendices

UK Ph D Theses, submitted during 2002

1. E Rodrigues (Bristol), *Measurement of Azimuthal Asymmetries in DIS at HERA*
2. S Boogert (Oxford), *Photoproduction of K_S^0 Mesons and Λ Baryons in ep collisions at ZEUS*

Talks on ZEUS and ZEUS-related physics given at major National or International Conferences

Talks at DIS02, Cracow, April 2002

The topics will also appear in the proceedings.

1. S. Boogert (Oxford), *Strange Hadron Production*.
2. A. Cooper-Sarkar (Oxford), *The Structure Function Working Group Summary*.
3. C. Gwenlan (UCL), *Multi-jet production in γ -p*.
4. M. Lightwood (UCL), *Virtual photons with charm*.
5. A. Lupi (Glasgow), *Photon Structure*.
6. S. Robins (Bristol), *D^* production in DIS*.

Other Talks

1. M. Wing (Bristol), *Jet energy scale determination*, Calorimetry, Pasadena, USA.
2. M. Wing (Bristol), *Physics at HERA – a review of recent results*. IoP HEPP Conference, Brighton, UK.
3. J. Cole (Bristol), *Gaps between Jets*, Workshop on low-x Physics, Antwerp, Belgium.
4. E. Rodrigues, (Bristol) *Jet physics and event shapes*, Moriond QCD, Les Arcs, Switzerland.
5. P. Bussey (Glasgow), *Jet Physics at HERA and Heavy Flavour physics at HERA*, XVI International Conference on Particles and Nuclei (PANIC02), Osaka, Japan October 2002.
6. D.H. Saxon (Glasgow), *Heavy Quark Production*, First International Conference on Frontier Science: Charm, Beauty and CP, Frascati, Italy October 2002.
7. A. Cooper-Sarkar (Oxford), *Uncertainties on Parton Distribution Functions from the ZEUS NLOQCD fit to Data on Deep Inelastic Scattering*, hep-ph/0205153, Int. Conf. on Advanced Statistical Techniques in Particle Physics, Durham, March 2002.
8. A. Cooper-Sarkar (Oxford), *ZEUS results on Structure Functions and Inelastic Cross-Section*, Review Talk and Discussion Leader's Summary, Workshop on Low-x Physics, Antwerp, September 2002.
9. R. Devenish (Oxford), *Low-x Physics at HERA*, hep-ex/0208043, Invited talk on behalf of ZEUS & H1 at the XXII Physics in Collision Conference, Stanford, CA, June 2002
10. M. Sutton (Oxford), *Jet production in deep inelastic scattering at HERA*, ICHEP02, July 2002, Amsterdam.
11. R. Hall-Wilton (UCL), *Charm and Beauty Production* Hadron Structure '02, Sep 2002, Herlany, Slovakia.
12. J.M. Butterworth (UCL), *HERA (p)review*, IPPP Workshop on TeV-scale physics, Cambridge, July 2002
13. A. Tapper (IC) *Workshop on Energy Calibration of the ATLAS Calorimeters*, July, 2002, Ringberg Castle, Germany.
14. K.Long (IC) *QCD at high energy (experiments)* ICHEP02, July 2002, Amsterdam.
15. K.Long (IC) *QCD at high energy* IPPP Workshop on TeV-scale physics, July 2002, Cambridge.
16. K.Long (IC) *ZEUS presentation at the open session* DESY PRC Meeting, April 2002.
17. K.Long (IC) *Polarisation measurements on e[±] beams* INSTR02, Novosibirsk, Russia.

ZEUS collaboration publications in 2002

- *Scaling violations and determination of α_s from jet production in γp interactions at HERA*, DESY-02-228, submitted to Phys. Lett. B
- *Measurement of subjet multiplicities in neutral current deep inelastic scattering at HERA and determination of α_s* , DESY-02-217, submitted to Phys. Lett. B
- *Measurement of event shapes in deep inelastic scattering at HERA*, DESY-02-198, submitted to Eur. Phys. J. C
- *Study of the azimuthal asymmetry of jets in neutral current deep inelastic scattering at HERA*, DESY-02-171, Phys. Lett. **B551** (2003) 3-4
- *Observation of the strange sea in the proton via inclusive phi-meson production in neutral current deep inelastic scattering at HERA*, DESY-02-184, submitted to Physics Letters B

- *Measurements of inelastic J/ψ and ψ' photoproduction at HERA*, DESY-02-163, submitted to Eur. Phys. J. C
- *Leading proton production in e^+p collisions at HERA*, DESY-02-142, submitted to Nucl. Phys. B
- *Measurement of high- Q^2 e^-p neutral current cross sections at HERA and the extraction of xF_3* , DESY-02-113, submitted to Eur. Phys. J. C
- *Inclusive jet cross sections in the Breit frame in neutral current deep inelastic scattering at HERA and determination of α_s* , DESY-02-112, submitted to Phys. Lett. B
- *A ZEUS next-to-leading-order QCD analysis of data on deep inelastic scattering*, DESY-02-105, accepted by Phys. Rev. D (DW8050)
- *Measurement of diffractive production of $D^{*\pm}$ (2010) mesons in deep inelastic scattering at HERA*, DESY-02-082, submitted to Phys. Lett. B
- *Measurement of proton-dissociative diffractive photoproduction of vector mesons at large momentum transfer at HERA*, DESY-02-072, submitted to Eur. Phys. J. C
- *Measurement of high- Q^2 charged current cross sections in e^-p deep inelastic scattering at HERA*, DESY-02-064, Physics Letters **B539** (2002) 197-217
- *Leading Neutron production in e^+p collisions at HERA*, DESY-02-039, Nucl. Physics **B637** (2002) 3-56
- *Measurement of the Q^2 and energy dependence of diffractive interactions at HERA*, DESY-02-029, Eur. Phys. J. **C25** (2002) 3, 169-187.
- *Exclusive photoproduction of J/Ψ mesons at HERA*, DESY-02-008, Eur. Phys. J. **C24** (2002) 3, 345-360.

Papers by ZEUS-UK authors on ZEUS-related topics

1. J.M. Butterworth, S Butterworth (UCL), *JetWeb: A WWW Interface and Database for Monte Carlo Tuning and Validation*, hep-ph/0210404.
2. J.M. Butterworth (UCL) et al, *KtJet: A C++ implementation of the K_T clustering algorithm*, hep-ph/0210022, submitted to Comp. Phys. Comm.
3. J.M. Butterworth (UCL) et al, *SNOWMASS 2001: JET ENERGY FLOW PROJECT*, hep-ph/0202207, Contributed to APS / DPF / DPB Summer Study on the Future of Particle Physics (Snowmass 2001), Snowmass, Colorado, June 2001.